AD-A106 776 OREGON GRADUATE CENTER BEAVERTON DEPT OF APPLIED PHY--ETC F/G 20/6
EFFECTS OF STRONG TURBULENCE ON SHORT WAVELENGTH LASER - EXPERI--ETC(U)
SEP 81 C M MCINTYRE

UNCLASSIFIED AFOSR-TR-81-0796 NL

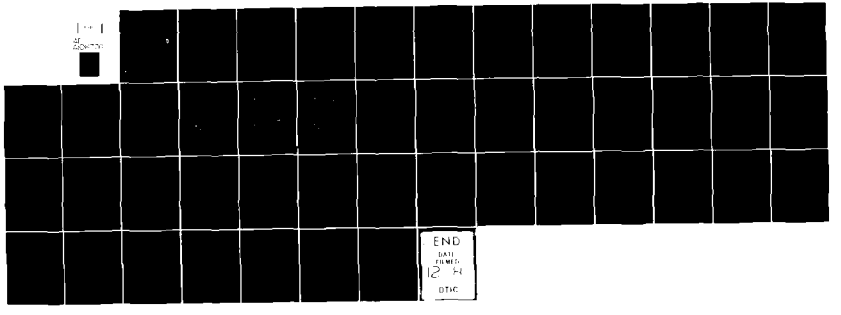

(12)

Effects of STRONG TURBULENCE [redacted] ON SHORT WAVELENGTH LASERS - EXPERIMENTAL DETERMINATION OF MEAN SQUARE WANDER ANGLE.

C. M. McIntyre

Department of Applied Physics and Electronic Science

Oregon Graduate Center

Beaverton, Oregon 97006

15 September 1981

Final Report.

Prepared for

AIR FORCE OFFICE OF SCIENTIFIC RESEARCH

Bolling Air Force Base, D.C. 20332

TABLE OF CONTENTS

LIST OF FIGURES

I. Introduction

The objective of this experimental study was to verify analytical work concerning some effects of strong turbulence on short wavelength lasers.[1] In particular, the r.m.s. wander angle of a transmitted laser beam, as a function of integrated path turbulence has been shown to increase to a maximum and then to decrease towards a constant value that is the same order as the diffraction limited spot size of the aperture in very strong turbulence. This means that an active correction for wander angle, applied at the transmitter, although useful at low to moderate levels of turbulence, is ineffective in increasing power density on the target for high levels of integrated path turbulence. An experimental measurement of the r.m.s. wander angle of a transmitted laser beam vs. integrated path turbulence in a simulated atmospheric path has been completed and the results are in qualitative agreement with the theory.

In order to measure the r.m.s. wander angle well into the saturation regime (the regime of very strong integrated path turbulence) under controlled, well documented, and repeatable conditions, an atmospheric turbulence simulation facility[2] was used. This facility consisted of a 10 gallon aquarium filled with ethanol that was heated at the bottom and cooled at the top to provide the thermal input resulting in the turbulence. This facility had been initially characterized, with respect to both the spatial spectrum of temperature fluctuations and the effects of the turbulence on optical propagation.

Prior to the wander angle measurements, this characterization was extended to include the spatial spectrum of temperature fluctuations as

a function of position in the medium. Spectra were recorded both above and below the optical center line as well as on the side in order to determine the uniformity of the turbulence. These measurements were made using a TSI model 1276 probe consisting of a 25 μm diameter glass fiber plated with platinum, with a length of 0.25 mm. This probe was used in conjunction with a Contel model MT-2 microthermal analyzer to digitally record the temperature fluctuations. The digital data was numerically processed to obtain the spectrum.

Wander angle measurements were made using a collimated He-Ne laser beam making one or more passes through the turbulence, and a centroid tracker to stabilize the output beam. The error signals generated by the tracker were digitized and numerically processed to obtain a measure of the wander angle. This measurement was made as a function of integrated path turbulence by varying both the path length (using multiple passes through the simulated turbulence) and by varying the thermal input.

There is an important aspect of the work that should be emphasized at the outset. Although the experimental arrangement provides a very good simulation of atmospheric turbulence, it is not the atmosphere, and there are certain differences that must be recognized. First of all, the spatial spectrum of temperature fluctuations in the laboratory generated turbulence does not have a well defined inertial-convective subrange corresponding to the Kolmogorov spectrum.[2] However, the significant point here is that the theoretical description of the spatial spectrum of index of refraction fluctuations in turbulent fluids[3] is

applicable both to the atmosphere and to the laboratory generated turbulence. Consequently, analytical descriptions of either the atmosphere or the laboratory generated turbulence are identical, although some of the parameters may differ. Evaluation of analytical results for the parameters of the laboratory generated turbulence has not been attempted. This makes the comparison of the experimental results presented in the next section with analytical results for the atmosphere a qualitative one. As is shown below, the significant features of the r.m.s. wander angle as a function of integrated path turbulence are common to both the analytical results as applied to the atmosphere and the experimental results as measured in the laboratory generated turbulence. In addition, although not specifically relevant to this work, two further differences between the atmospheric and laboratory generated turbulence are noted. High integrated path turbulence in the laboratory (deep into the saturation regime) is obtained with path lengths on the order of 2 meters. This is much different than the multikilometer path lengths required in the atmosphere. Further, the time scale of the fluctuations in the laboratory generated turbulence is much slower than in the atmosphere.

II. Results

A. Uniformity of Turbulence

The initial task of this program was to investigate the uniformity of the laboratory generated turbulence in the ethanol. This was accomplished by measuring the spatial spectrum of temperature fluctuations at several positions throughout the tank, both within and around the volume

utilized by the multiple pass optical beam. The spatial spectrum at each position was measured by recording the temperature fluctuations in the ethanol using a moving probe. The data was recorded digitally and then processed by taking a discrete Fourier transform of the time records. At each location in the tank, on the order of 60 time records were obtained. These time records were then processed separately and averaged to give the final spatial spectra presented here. A comparison of the spectra at different locations indicates uniform turbulence throughout the tank.

The measurements utilized a thermal probe with dimensions of 25 μm diameter, and 0.25 mm length. It is presumed that spatial scales on this order were resolvable. The probe constituted one leg of a resistance bridge, the output of which was amplified, converted to digital form and then recorded on magnetic tape. The probe was moved through the medium at a velocity of 1 cm per second during the recording, with a total travel of approximately 10 cm. A single time record consisted of one pass of the probe over this 10 cm length. The time during the return of the probe to the starting point was not utilized in taking data. (More properly, although data was taken during the return of the probe, only data taken while the probe was in motion in one direction was utilized.) A typical measurement consisted of 60 round trips of the probe, giving 60 one way time records of the temperature fluctuations.

Since the data was processed in digital form, care was taken to avoid both aliasing and leakage. The amplified analog signal from the thermal probe was passed through a low pass filter with a 3 db bandwidth of 50 Hz. This cutoff frequency was chosen to correspond to that of the 1.0

millisecond sampling time, in order to minimize the effects of aliasing. Although the results indicated no quantitative difference between spectra with and without the filter it was used initially to determine whether or not some "spurious" signals were the result of aliasing. The filter also was useful in reducing the magnitude of a 60 Hz spike that appeared in the spatial spectra.

The analog output of the 50 Hz low pass filter was converted to digital form and then recorded on magnetic tape. This digital time record was then used to find the spatial spectrum of the temperature fluctuations. The digital time record was first multiplied by a Hanning window to reduce the effects of leakage and then a fast Fourier transform (FFT) was taken. The spatial spectrum was then found as the modulus squared of the FFT. This processing was done for each of approximately 60 time records and these 60 spectra were averaged to obtain the spatial spectra presented here.

In addition, a "noise spectrum" was obtained in a similar manner. With the thermal input to the tank turned off, 60 records of the temperature fluctuations were recorded using the anti-aliasing filter. This data was processed using a Hanning window, with the resulting spectra averaged over the 60 records to obtain an average noise spectrum. This noise spectrum was subtracted from the averaged thermal spectra to obtain the final results.

Figures 1 through 4 illustrate the spectra obtained using a 20 millisecond sampling interval. Figure 1 is the spectrum of temperature fluctuations obtained by averaging 60 time records with the probe moving

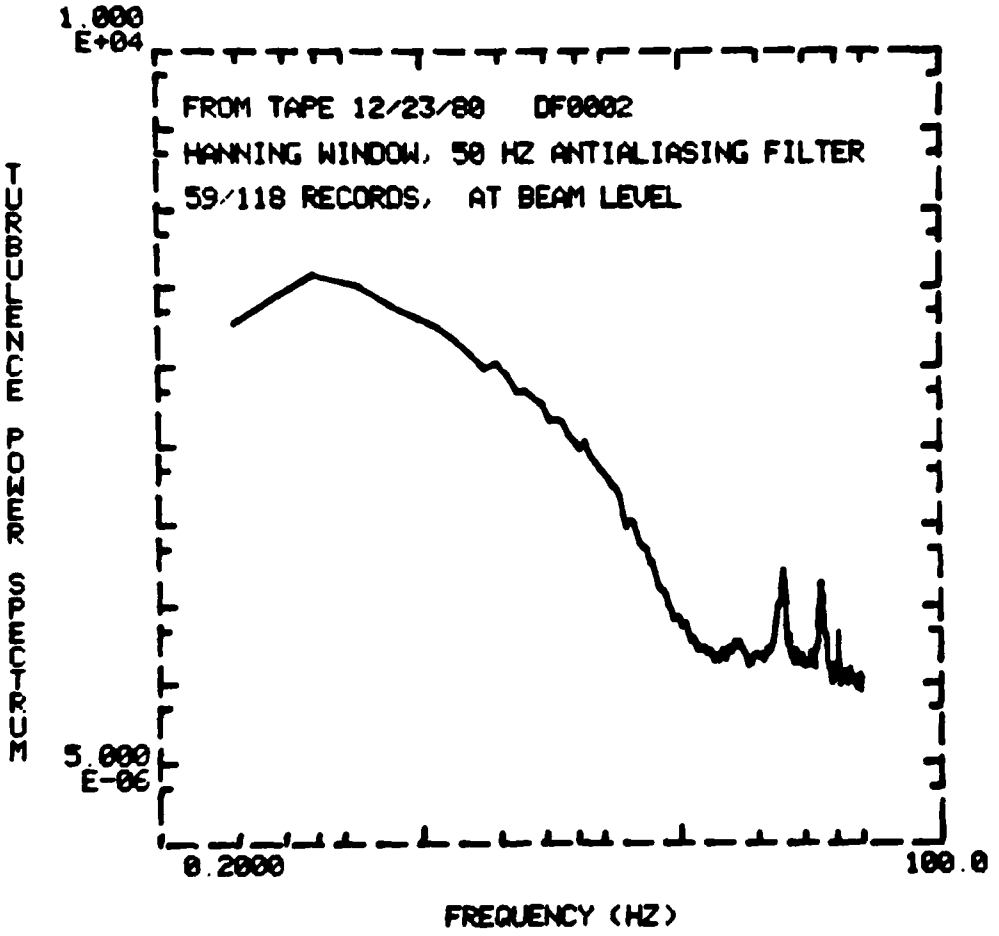

Figure 1. Spatial spectrum of temperature fluctuations on the optical center line of the tank. The ordinate is an arbitrary scale indicating the magnitude of the spectrum. The abscissa is a temporal frequency that is related to the spatial frequency through the velocity of the thermal probe (1 cm/sec) Spatial frequency = (2π/1 cm per sec) × (Temporal frequency).

along the optical center line of the tank. In the following computer generated curves, the ordinate is an arbitrary scale indicating the strength of turbulence. The abscissa is a temporal frequency that is related to the spatial frequency. Spatial frequency may be obtained by multiplying the abscissa by 2π and dividing by 1 cm/sec, the velocity of the probe. For reference, 10 Hz corresponds to $\kappa = 62.8\ cm^{-1}$ i.e., to a scale size of approximately 1 mm where κ is the spatial wave number. Note that the energy is down by somewhat more than four orders of magnitude by $\kappa = 100\ cm^{-1}$ ($\sim$ 16 Hz on the graph). At 40 Hz, there is a small spike in the spectrum that results from 60 Hz interference that is aliased in to the spectrum. There are also two peaks that appear in the spectrum at approximately 25 Hz and 35 Hz. These peaks occurred in all temperature spectra obtained during the month of December (in subsequent measurements during March of the following year, both the magnitude and position of these peaks were extremely variable, unlike those shown here). These peaks did not appear in the noise spectra and remain unexplained.

Figure 2 is the average noise spectrum recorded at the optical center line of the tank and averaged over 60 records. Note that with the exception of the first point, it is flat out to 50 Hz and the only feature is the aliased 60 Hz. Note in particular that the spurious peaks observed in the temperature power spectrum do not appear.

Figure 3 is identical to Figure 1 but it has the noise of Figure 2 subtracted. It is plotted using points rather than a solid line since in the neighborhood of 20-40 Hz, the difference between the temperature

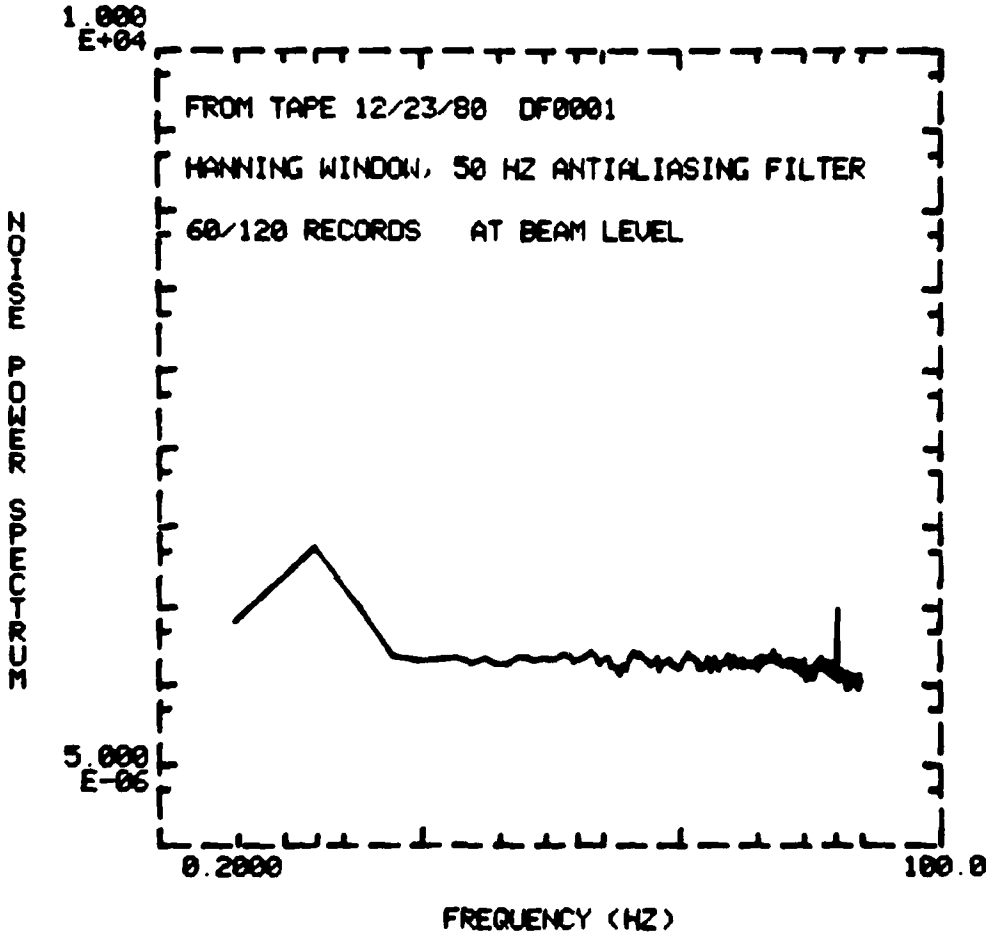

Figure 2. Noise spectrum recorded on the optical center line of the tank with the thermal input to the tank turned off. Abscissa as in Figure 1.

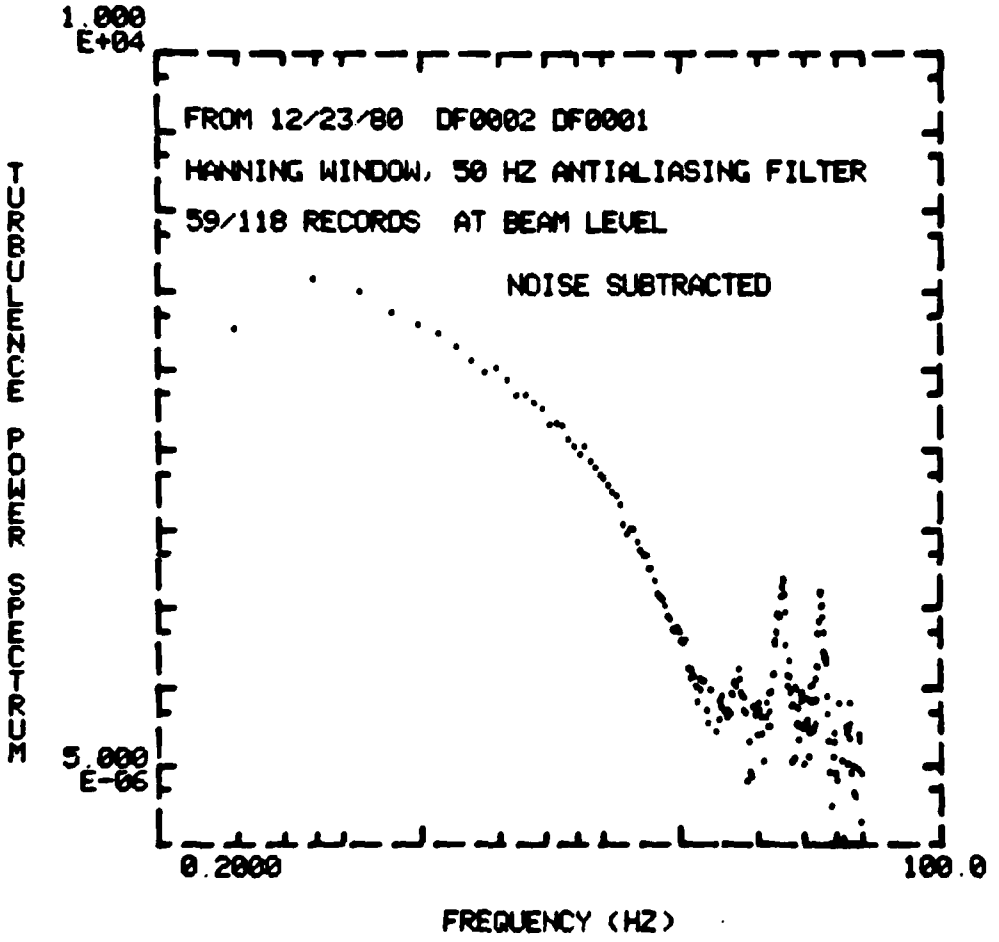

Figure 3. Spatial spectrum of temperature fluctuations on the optical center line of the tank from Figure 1 with the noise spectrum from Figure 2 subtracted. Ordinate and abscissa as in Figure 1.

spectrum and noise spectrum was extremely small in some cases. This resulted in an unclear plot when a line curve was used. Subtracting the noise leaves a spectrum with the energy down by 5 orders of magnitude at $\kappa \sim 100$ cm^{-1} (approximately 16 Hz). The peaks at 25 and 35 Hz are clearly visible.

Figure 4 is an average temperature spectrum taken 2.5 cm below the optical center line and shows an identical spectrum to that of Figure 1. Spectra obtained with the probe 2.5 cm above the optical center line also show identical spectra.

Figures 5 through 7 show a similar series of spectra taken in a horizontal plane including the optical center line and using a 10 millisecond sampling interval. These spectra were taken approximately two and one-half months after those in Figures 1 through 4. Figure 5 is a spectrum taken from the optical center line of the tank and exhibits the same features as the previous spectra except that the unexplained peaks are missing. Figure 6 is the spectrum taken halfway between the optical center line and the wall of the tank approximately 6 cm from the optical center line, and Figure 7 is the spectrum taken at 1 cm from the wall in the same horizontal plane as the optical center line. From the similarity of these spectra, it is concluded that the turbulence is uniform throughout the volume of the tank utilized by the optical beam. Although the "edge effects" must be present at the wall, they contribute only a small amount to the overall turbulence.

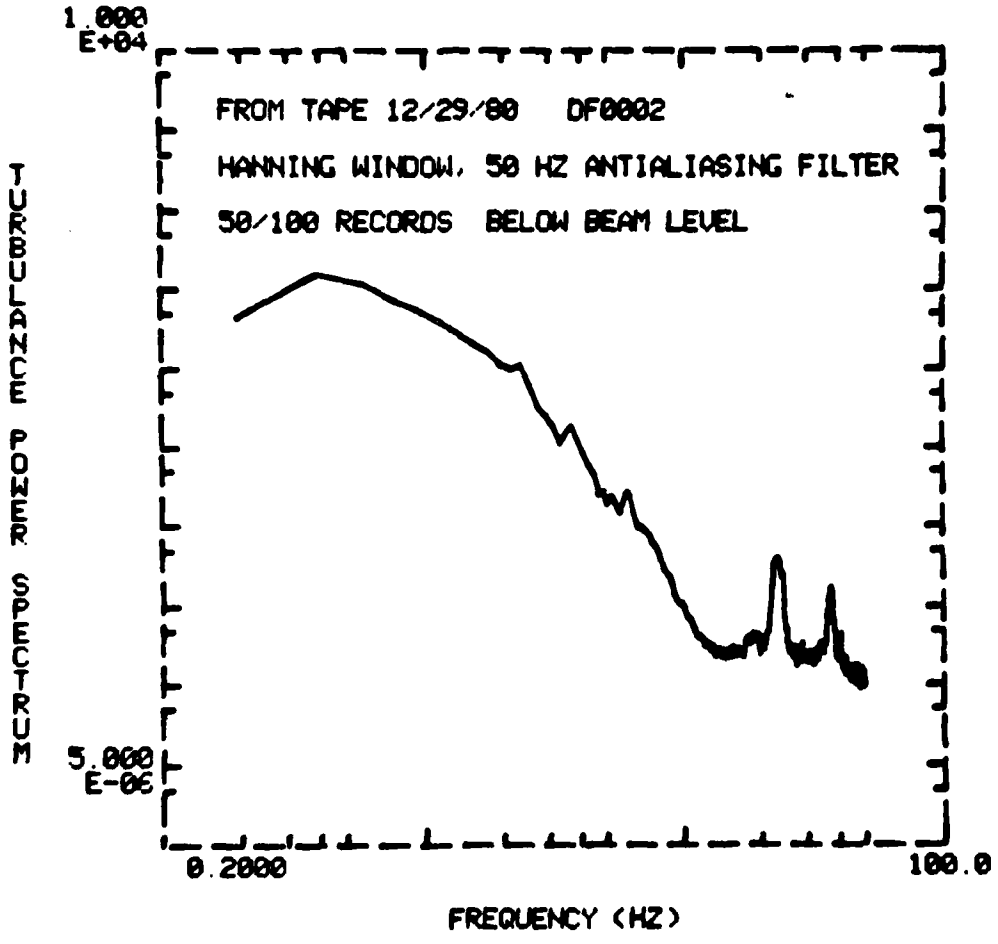

Figure 4. Spatial spectrum of temperature fluctuations 2.5 cm below the optical center line. Ordinate and abscissa as in Figure 1.

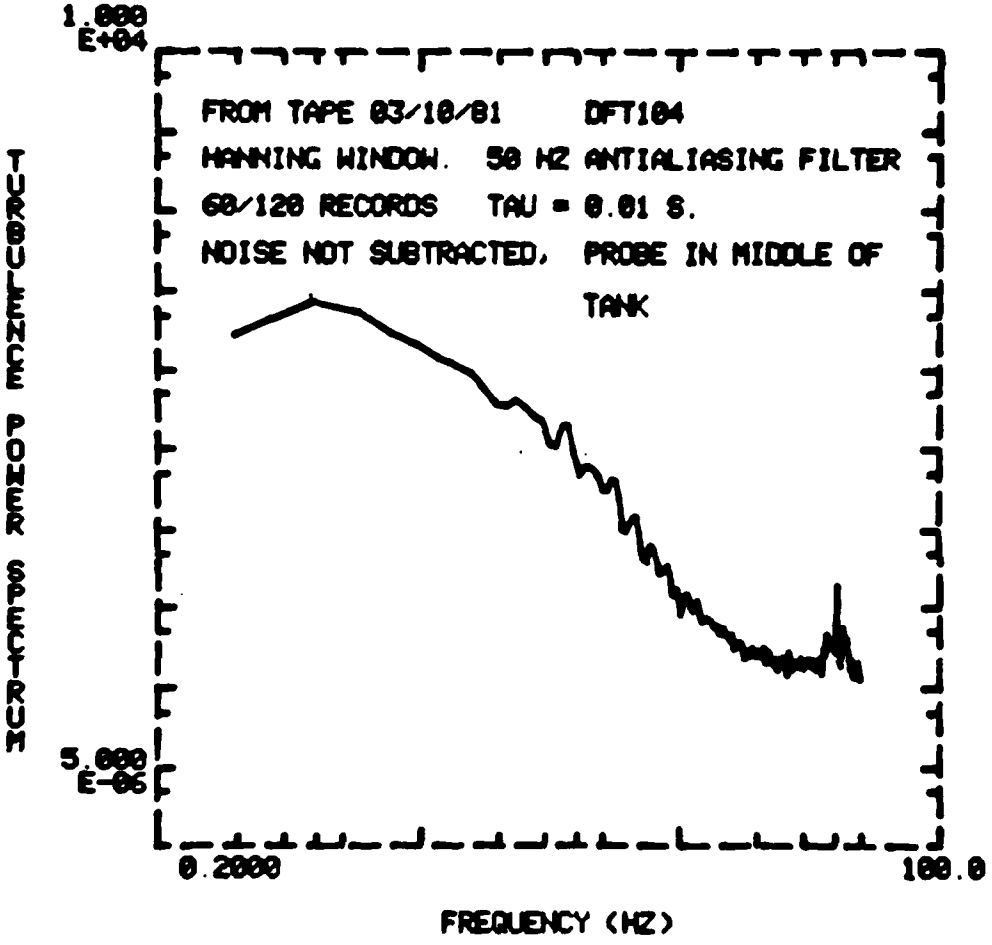

Figure 5. Spatial spectrum of temperature fluctuations on the optical center line of the tank. Ordinate and abscissa as in Figure 1.

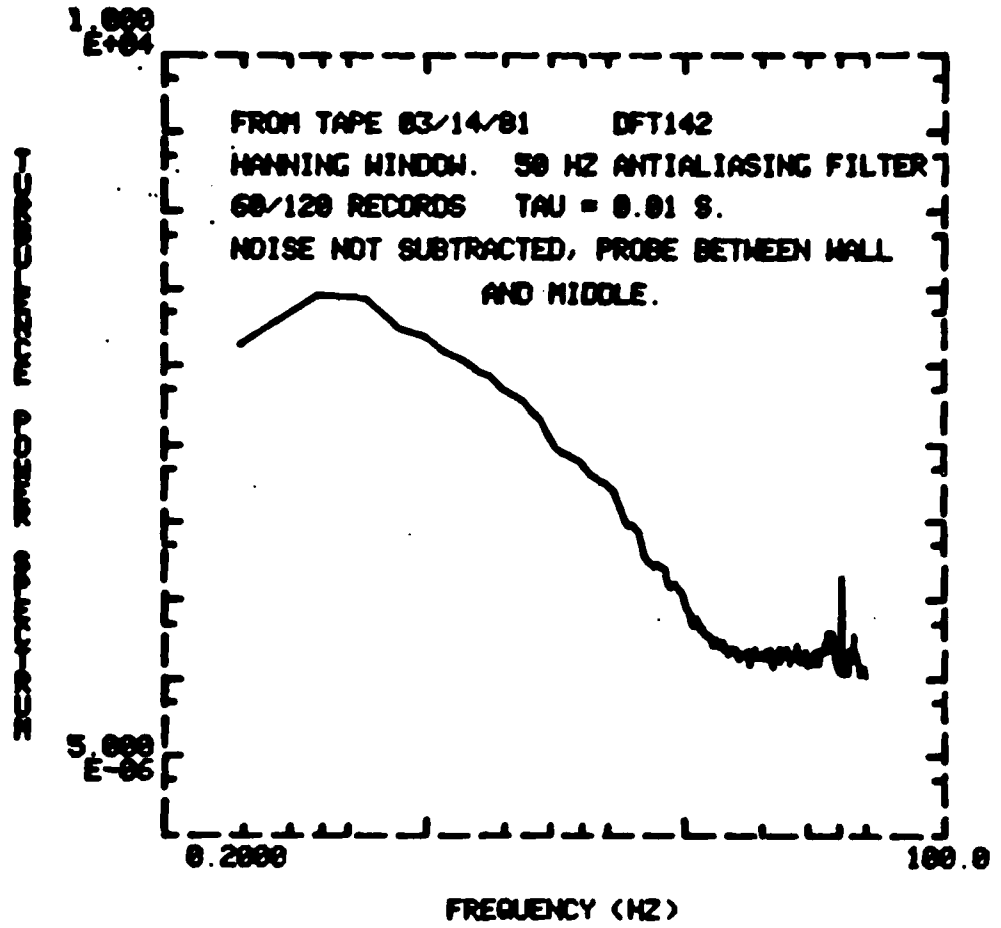

Figure 6. Spatial spectrum of temperature fluctuations in the horizontal plane including the optical center line, halfway between the center line and the wall. Ordinate and abscissa as in Figure 1.

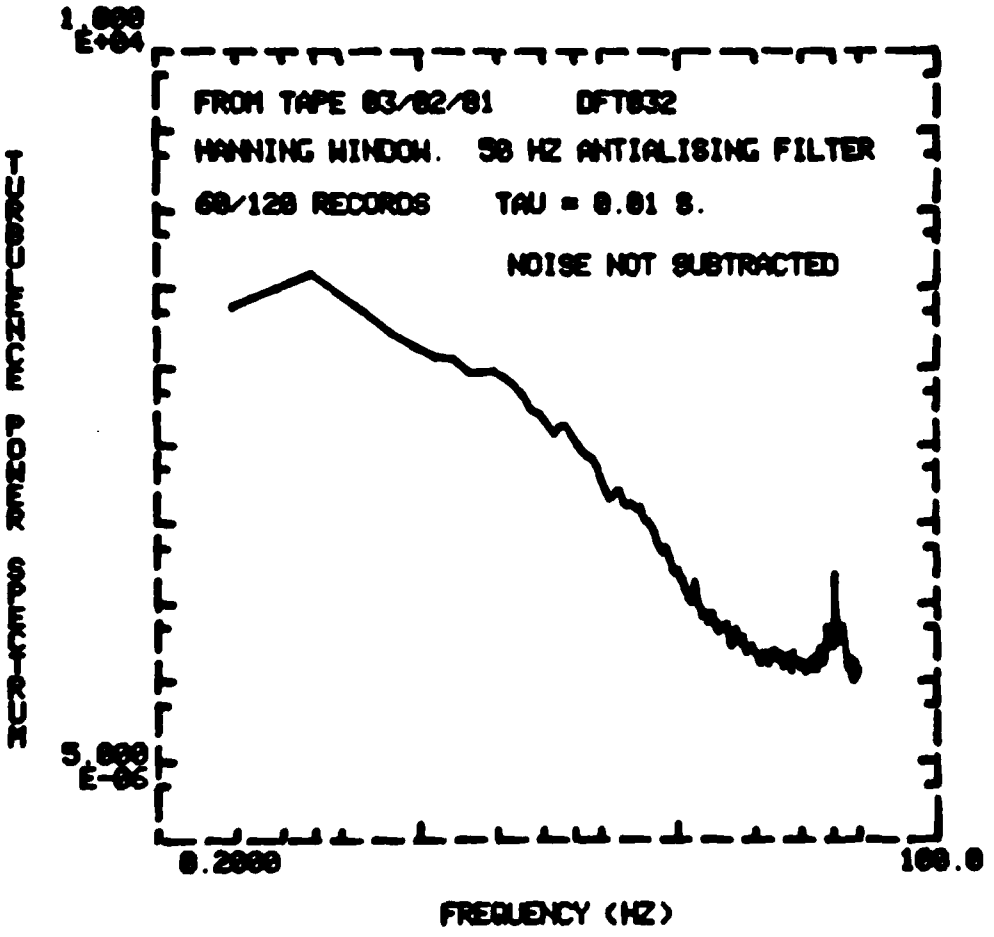

Figure 7. Spatial spectrum of temperature fluctuations in the horizontal plane including the optical center line, 1 cm from the wall of the tank. Ordinate and abscissa as in Figure 1.

B. Wander Angle

The far field wander angle of a collimated beam propagating through a simulated atmospheric turbulence as a function of integrated path turbulence was measured using a centroid tracker and was found to be in qualitative agreement with analytical results.[1] The wander angle measurements were made with two geometries. The first was with the collimated HeNe laser beam making three passes through the tank. It was found, as reported below, that through the highest levels of integrated path turbulence obtainable with the experimental arrangement, the magnitude of the r.m.s. wander angle continued to increase with turbulence strength. The geometry was then changed so that the laser beam made 5 passes through the simulated turbulence. As the turbulence strength was increased, the r.m.s. wander angle increased initially, reached a maximum and then began to decrease. With the exception of the angle measurements, the parameters utilized in the results below were those obtained in the previous simulation work.[2]

The angle measurements were obtained utilizing the experimental configuration shown in Figure 8. A centroid tracker, consisting of two mirrors that could each be electrically driven to vary the angle of the emerging beam, a 4-element quadrant detector, and electronics to drive the mirrors in response to error signals from the detector, was used to measure the angle of arrival of the beam emerging from the turbulent medium. The General Scanning model 102 deflection mirrors were arranged to provide orthogonal angular deviations of the emerging beam. The UDT PIN SPOT 4 quadrant detector divides the image plane into four quadrants

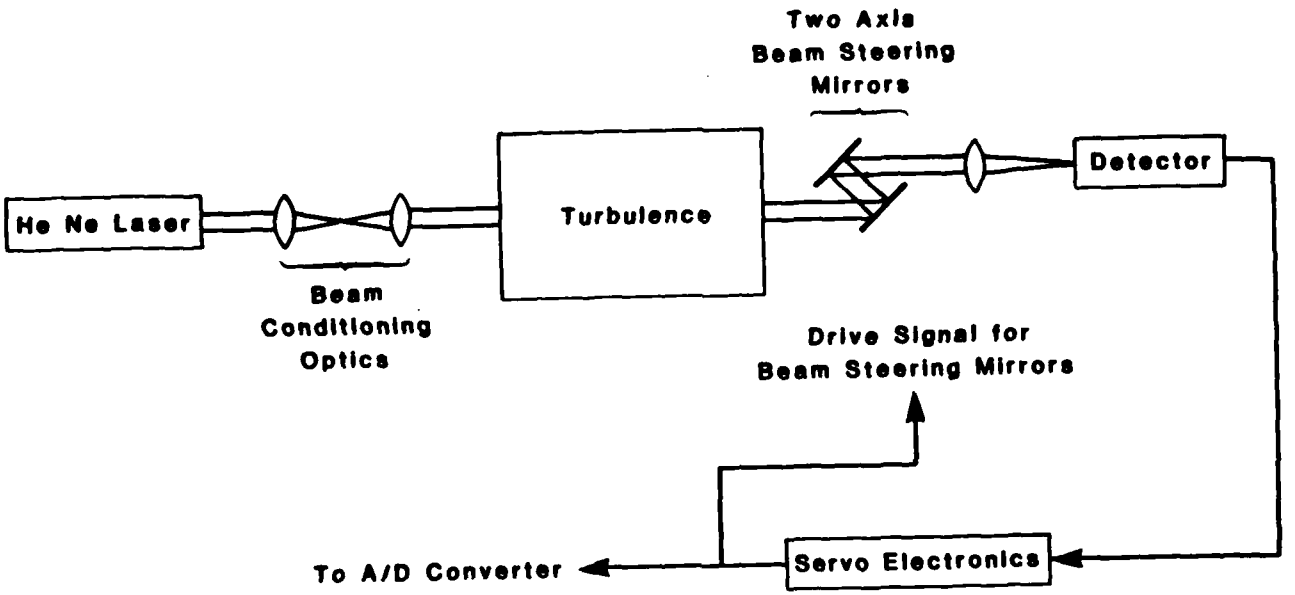

Figure 8. Schematic of the experimental arrangement for measuring r.m.s. wander angle.

and detects the intensity of the light incident on each of the quadrants. Appropriate combinations of the output signals may be used to determine the position of the centroid of the incident light with reference to the center of the detector. The up-down, left-right signals thus generated are used as error signals that drive the mirrors to reposition the centroid of the light at the center of the detector. The error signals are consequently a measure of the angular deviation of the beam from the optical center line. The system was calibrated by using an identical General Scanning mirror at the input to the tank, to introduce known angles. These angles were measured with the centroid tracker and the results allowed calibration of the angle measurement system.

Results were obtained for two separate path lenths; 1.5 meters corresponding to three passes through the tank, and 2.5 meters corresponding to 5 passes through the tank. For each path length, the thermal input to the turbulence was varied from 200 watts to 600 watts in steps of 100 watts. Higher input powers were avoided because the temperatures reached at the heater elements near the base of the tank began to initiate damage to the structure. For each path length, and at each input power level, wander angle measurements were made by digitizing the error signals from the centroid tracker and recording these on magnetic tape. In each case, 60 time records consisting of 512 samples of the analog signal were obtained. This data was then numerically processed to obtain the average variance or mean square wander angle, and the power spectrum of angular fluctuations by determining the modulus squared of the Fourier transform (using the FFT of the windowed data)

averaged over the 60 records. The results of this experiment are displayed in Figure 9. The ordinate is the measured r.m.s. wander angle, and the abscissa is $\tilde{C}_n^2$, a dimensionless parameter describing the strength of turbulence in the tank (defined in Ref. 2), and which may be compared to the usual structure parameter C_n^2. The values of $\tilde{C}_n^2$ were obtained from the heater power and Figure 10 of Ref. 2. Note at the shortest path length (1.5 meters corresponding to three passes through the tank), the r.m.s. wander angle increases monotonically with turbulence strength. At 2.5 meters, the r.m.s. wander angle increases initially, reaches a peak, and then decreases as turbulence strength increases. This is in agreement with the analytical results of Ref. 1. To illustrate the similarity of the results, the curves of Ref. 1 are replotted in Figure 10 for a wavelength of 0.651 μm, zero obscuration ratio, and path lengths of 1 and 10 kilometers. As in the experimental data of Figure 9, the r.m.s. wander angle increases monotonically for the shorter path length, and reaches a peak and decreases with increasing turbulence strength for the longer path length.

The numerical results utilized in generating the 2.5 meter path length curve in Figure 9 are collected in the Appendix and include the mean and variance of the wander angle for each of the 60 records per data point along with the associated power spectrum.

It may be pointed out that the curves of Ref. 1 indicate a peak in the r.m.s. wander angle which occurs in each case considered at a value of the log irradiance variance calculated in the Rytov approximation that is approximately constant. Using the expression for a locally isotropic medium[4]

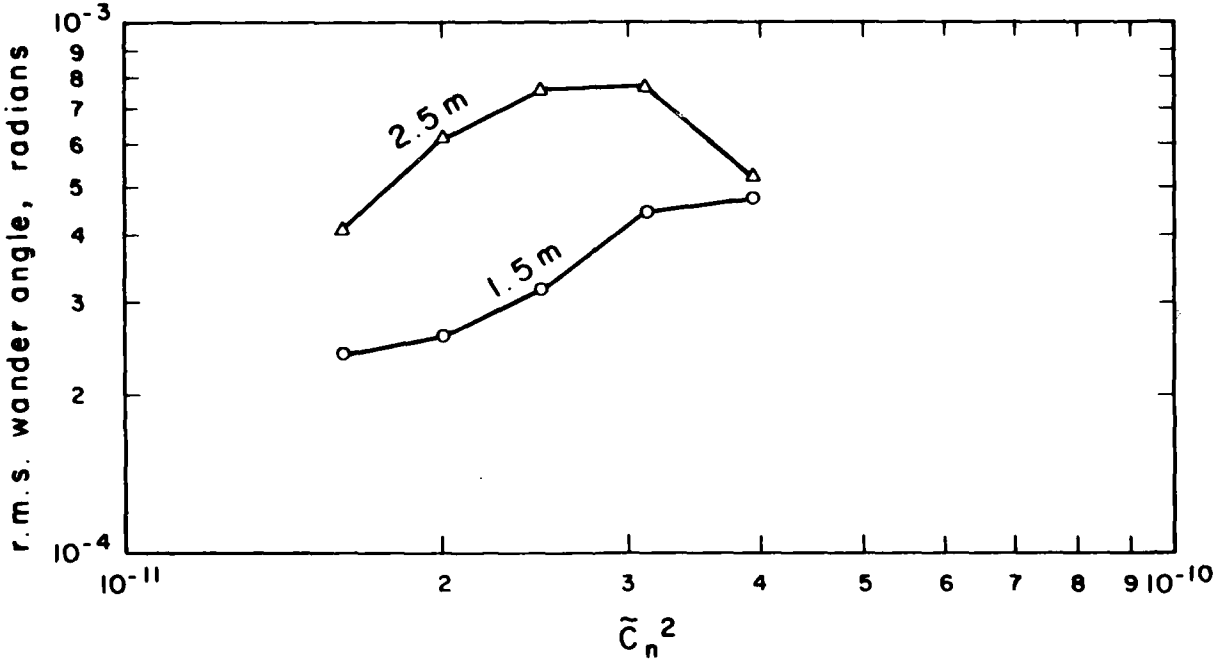

Figure 9. Experimental r.m.s. wander angle vs strength of turbulence for path length of 1.5 meters and 2.5 meters in the tank. $\tilde{C}_n^2$ from Ref. 2.

$$\sigma_{\ell nI}^2 = 1.23\, C_n^2\, k^{7/6}\, L^{11/6}$$

and the curves of Ref. 1, the peak occurs at about

$$\sigma_{\ell nI}^2 \approx 7.$$

This particular value is calculated using Figure 20 of Ref. 1 where $C_n^2 = 1.0 \times 10^{-14}$, $\lambda = 0.651$ μm, and $L = 4$ km. For comparison with the experimental results, the peak in the r.m.s. wander angle occurs at a value of the log irradiance variance calculated in the Rytov approximation of approximately $\sigma_{\ell nI}^2 = 135$ using the expression of Ref. 2. The numerical discrepancies between the experimental results in the ethanol, and the analytic results in the tank may be reconciled by applying the theory developed in Ref. 2 to the parameters associated with the turbulence in ethanol. This has not been attempted.

III. Conclusions

In order to obtain quantitative comparisons between analytic results and experiments in the simulated atmospheric turbulence utilized in this investigation, the general theory must be applied using the parameters of the simulated turbulence. In particular, any analytical calculations must utilize the Hill spectrum[1] of index of refraction fluctuations (or some other appropriate model), and in addition must recognize the dramatic difference in path lengths, required to obtain a given value of integrated path turbulence, between the turbulence developed in ethanol, and that in the atmosphere. Unfortunately, that was not within the scope of this work and the comparisons are necessarily qualitative.

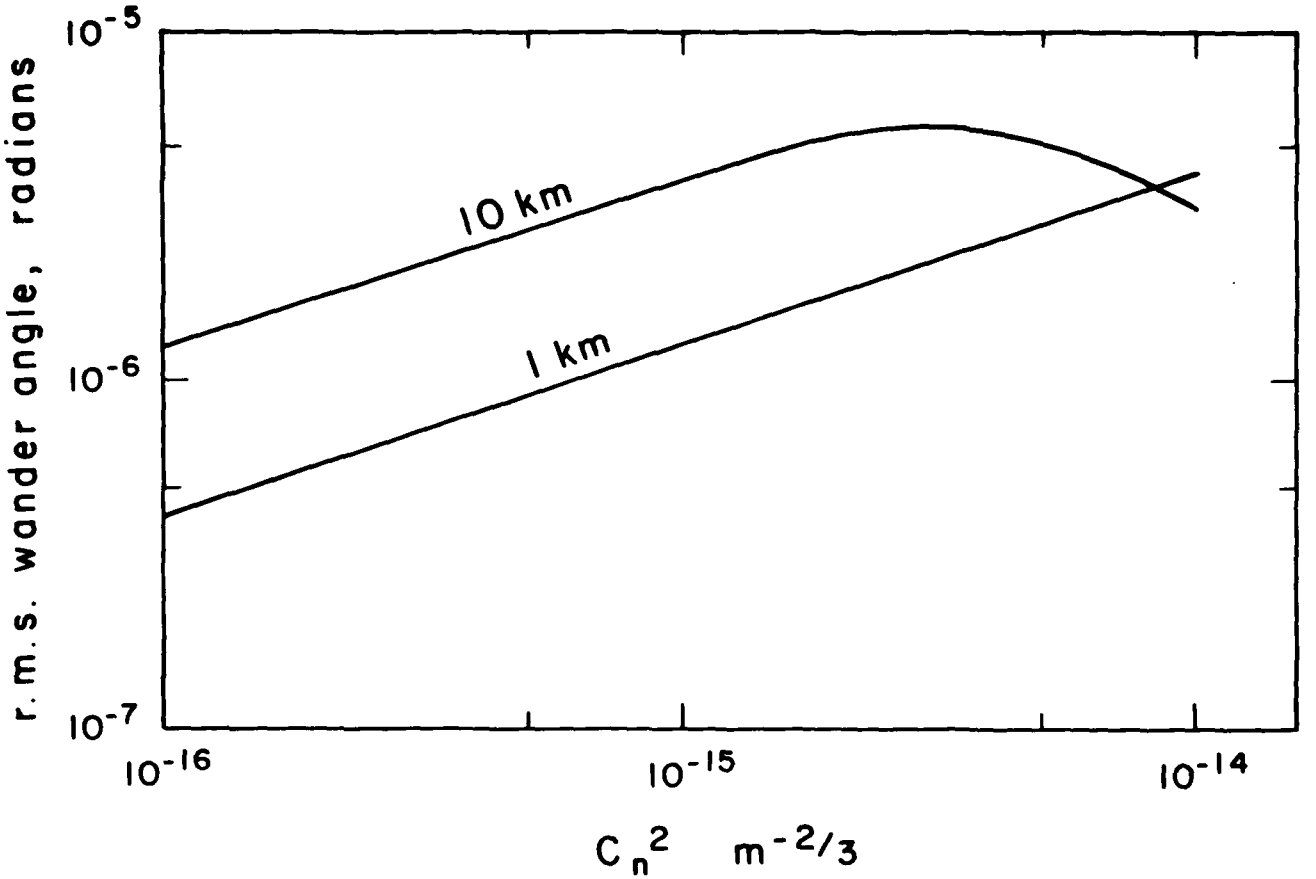

Figure 10. Theoretical r.m.s. wander angle vs strength of turbulence for path length of 1 km and 10 km in the atmosphere. This figure is derived from the results presented in Ref. 1.

Recognizing this limitation, it is apparent that the analytical results of Ref. 1 and the experimental results presented here are in qualitative agreement. Specifically, the r.m.s. wander angle in the far field of a transmitted laser increases initially with integrated path turbulence, reaches a peak, and then decreases. This peak occurs in the saturation regime where $\sigma_{\ell nI}^2 \gtrsim 10$ in the Rytov approximation and further increases in integrated path turbulence (due to increased path length, higher turbulence strength, or shorter wavelength) results in a decrease in the r.m.s. wander angle. One implication of this is that angular corrections applied to a transmitted wavefront become increasingly less effective in increasing power density on target as integrated path turbulence increases beyond the peak of angular fluctuations. This may be important in considerations involving short wavelength lasers where the saturation regime is encountered at relatively modest path lengths.

As an additional task, it was found that the spatial spectrum of temperature fluctuations is extremely uniform throughout the laboratory generated turbulence. This indicates that the laboratory generated turbulence supplies a uniform medium with properties closely associated with turbulence in the atmosphere that may be utilized both for verifying theoretical results and for testing actual systems.

DATA SET #1

Identification # 4/3/81 - DFA031

Input Power: 200 watts

Sampling Time: 20 milliseconds

ANGLE DATA VALUES ARE IN RADIANS.

ANGLE DATA VALUES ARE IN RADIANS.
NOISE SUBTRACTED = F, HANNING WINDOW = T.
ENSEMBLE POWER SERIES COMPUTED AT 15:10:02 ON MON, APR 06 1981
FROM DATA ON TAPE DATED: 04/03/81
SAMPLING INTERVAL IS: 0.0200 SECONDS.
60 RECORDS OUT OF 60 WERE USED,
AND 0 WERE BAD
THE AVERAGE VARIANCE FOR ALL RECORDS IS: 0.168962060E-06

RECORD	MEAN	VAR
1	0.0044824	0.582418025E-07
2	0.0047981	0.173540286E-06
3	0.0041184	0.138451924E-06
4	0.0044063	0.534130209E-06
5	0.0037848	0.627129262E-07
6	0.0039187	0.517324494E-07
7	0.0039230	0.749221130E-07
8	0.0042992	0.999176269E-07
9	0.0039330	0.290624982E-07
10	0.0040393	0.239859958E-06
11	0.0037686	0.185282154E-07
12	0.0039560	0.491353376E-07
13	0.0044192	0.129640426E-06
14	0.0033629	0.297022268E-06
15	0.0041348	0.118448696E-06
16	0.0041178	0.951941388E-07
17	0.0037712	0.159169645E-06
18	0.0037475	0.736754657E-07
19	0.0036592	0.171795904E-06
20	0.0038873	0.255767077E-06
21	0.0038934	0.802489666E-07
22	0.0039042	0.514499519E-07
23	0.0039719	0.234231514E-07
24	0.0041262	0.109045217E-06
25	0.0043401	0.221266191E-06
26	0.0047984	0.207884284E-06
27	0.0039882	0.219685489E-06
28	0.0041707	0.249841378E-06
29	0.0040018	0.352385314E-06
30	0.0039723	0.522933306E-06
31	0.0039711	0.265551648E-06
32	0.0036677	0.190566709E-06
33	0.0042655	0.166703359E-06
34	0.0042150	0.956639497E-07
35	0.0042090	0.546123644E-07
36	0.0038275	0.748417364E-07
37	0.0033596	0.882465514E-07
38	0.0040232	0.473939735E-06
39	0.0034325	0.313779708E-06

40	0.0040927	0.167847674E-06
41	0.0035927	0.141750405E-06
42	0.0032188	0.150116268E-06
43	0.0037228	0.147547411E-06
44	0.0038502	0.995430867E-07
45	0.0035096	0.145857854E-06
46	0.0041113	0.148216600E-06
47	0.0038470	0.144996420E-06
48	0.0034605	0.151737652E-06
49	0.0043639	0.198704953E-06
50	0.0042119	0.691755872E-06
51	0.0039612	0.311735675E-06
52	0.0034847	0.581679274E-07
53	0.0034216	0.390865225E-07
54	0.0036865	0.294760753E-06
55	0.0038709	0.153946264E-06
56	0.0038991	0.585423265E-07
57	0.0036354	0.640122709E-07
58	0.0036218	0.463377887E-07
59	0.0039033	0.119032691E-06
60	0.0039814	0.191031262E-06

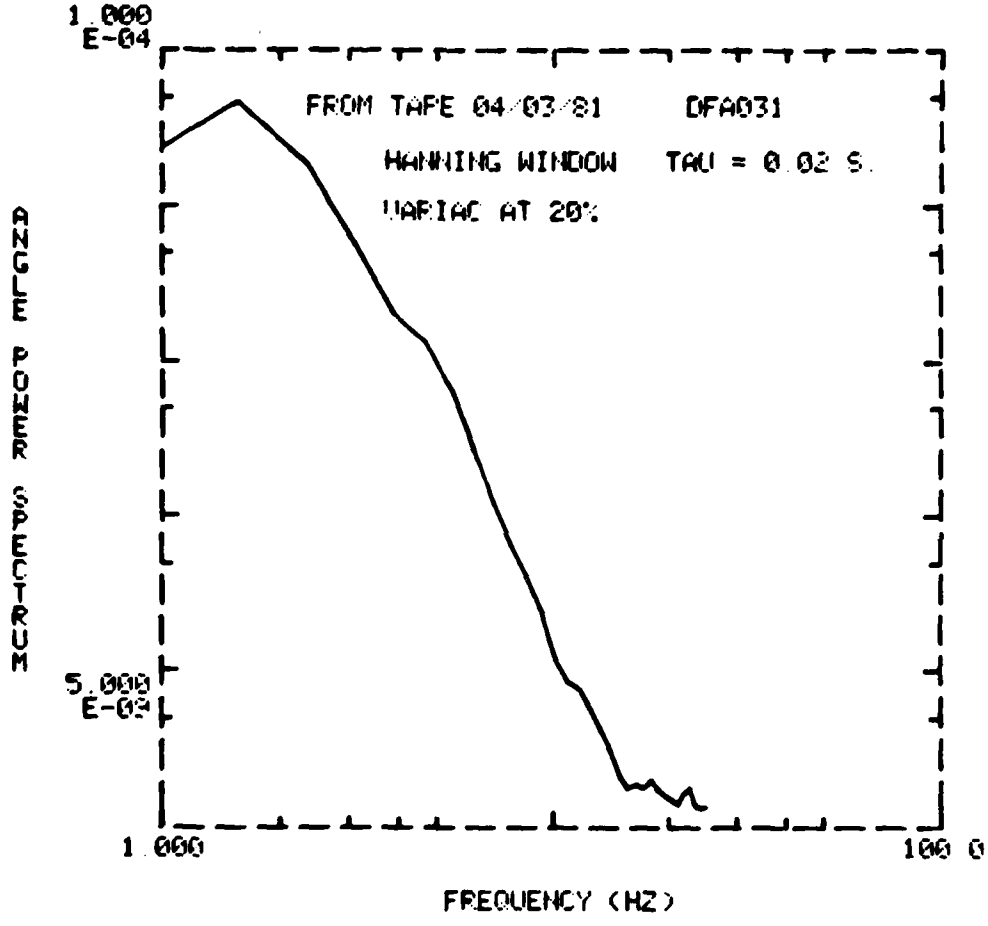

Figure A-1. Power spectrum of angle fluctuations for an input power of 200 watts.

DATE SET #2

Identification # 4/10/81 - DFA101

Input Power: 300 watts

Sampling Time: 20 milliseconds

ANGLE DATA VALUES ARE IN RADIANS. BEAM MADE 5 PASSES. VARIAC @ 30%

ANGLE DATA VALUES ARE IN RADIANS. BEAM MADE 5 PASSES. VARIAC @ 30%
X SCALE FACTOR WAS: 29.254E-06 RAD/UNIT
Y SCALE FACTOR WAS: 18.161E-06 RAD/UNIT
NOISE SUBTRACTED = F, HAMMING WINDOW = T.
ENSEMBLE POWER SERIES COMPUTED AT 15:57:05 ON MON, APR 13 1981
FROM DATA ON TAPE DATED: 04/10/81
SAMPLING INTERVAL IS: 0.0200 SECONDS.
60 RECORDS OUT OF 60 WERE USED,
AND 0 WERE BAD
THE AVERAGE VARIANCE FOR ALL RECORDS IS: 0.37422955E-06

RECORD	MEAN	VAR
1	0.0030947	0.79855169E-06
2	0.0034861	0.18724344E-06
3	0.0038032	0.22058989E-06
4	0.0035354	0.35904196E-06
5	0.0035874	0.32922156E-06
6	0.0031070	0.54915995E-06
7	0.0045977	0.38625624E-06
8	0.0048178	0.56594478E-06
9	0.0046550	0.30062494E-06
10	0.0039371	0.12525635E-06
11	0.0036720	0.16427469E-06
12	0.0033391	0.10700057E-06
13	0.0034228	0.93173625E-07
14	0.0034016	0.35321767E-06
15	0.0036853	0.31614664E-06
16	0.0039710	0.35037766E-06
17	0.0040284	0.22713251E-06
18	0.0039797	0.29167756E-06
19	0.0035255	0.15231927E-06
20	0.0039703	0.15675701E-06
21	0.0042463	0.53286746E-06
22	0.0035064	0.28373233E-06
23	0.0027408	0.24566770E-06
24	0.0037330	0.90758010E-06
25	0.0037833	0.25387652E-06
26	0.0040570	0.18890017E-06
27	0.0045165	0.68052156E-06
28	0.0040886	0.10236929E-06
29	0.0037144	0.24957381E-06
30	0.0036257	0.13215046E-06
31	0.0039389	0.34374060E-06
32	0.0035196	0.36291385E-06
33	0.0036409	0.37988905E-06
34	0.0042172	0.46487190E-06
35	0.0039125	0.11608359E-05
36	0.0035415	0.14326073E-06

37	0.0036534	0.3706752195E-06
38	0.0037358	0.1388744988E-06
39	0.0040655	0.1693034900E-06
40	0.0046548	0.9332286193E-06
41	0.0039226	0.2817066662E-06
42	0.0038767	0.5753292956E-06
43	0.0039175	0.3508899138E-06
44	0.0032163	0.3794197606E-06
45	0.0035490	0.9227117066E-06
46	0.0039986	0.1240073463E-06
47	0.0035297	0.2163343426E-06
48	0.0034344	0.1813243396E-06
49	0.0040313	0.2606918776E-06
50	0.0040402	0.8730772556E-07
51	0.0037993	0.3307115436E-06
52	0.0040197	0.4853791326E-06
53	0.0041952	0.3418486336E-06
54	0.0043102	0.2081228566E-06
55	0.0043481	0.1829997136E-06
56	0.0047401	0.1127708406E-05
57	0.0036659	0.1265825186E-05
58	0.0046175	0.4774986756E-06
59	0.0041715	0.2035645826E-06
60	0.0038368	0.3676447026E-06

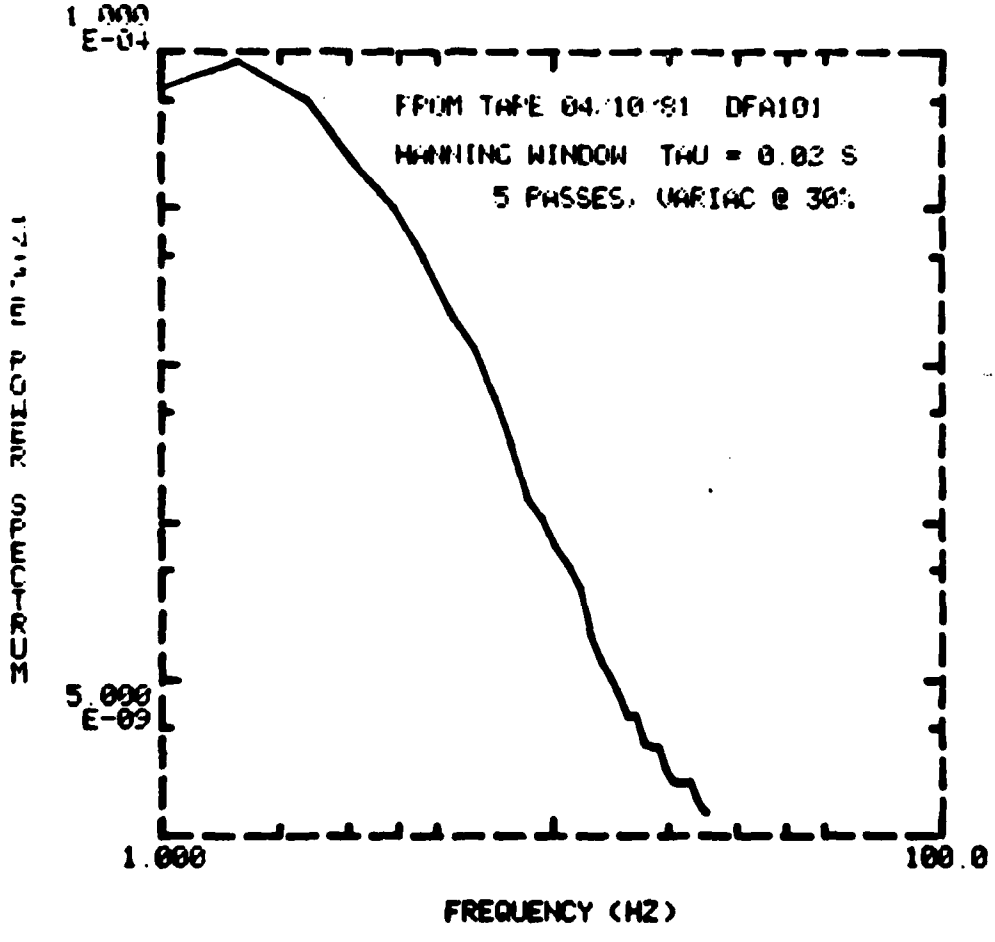

Figure A-2. Power spectrum of angle fluctuations for an input power of 300 watts.

DATE SET #3

Identification # 4/3/81 - DFA032

Input Power: 400 watts

Sampling Time: 20 milliseconds

ANGLE DATA VALUES ARE IN RADIANS.

ANGLE DATA VALUES ARE IN RADIANS.
NOISE SUBTRACTED = F, HANNING WINDOW = T.
ENSEMBLE POWER SERIES COMPUTED AT 15:15:14 ON MON, APR 06 1981
FROM DATA ON TAPE DATED: 04/03/81
SAMPLING INTERVAL IS: 0.0200 SECONDS.
60 RECORDS OUT OF 60 WERE USED,
AND 0 WERE BAD
THE AVERAGE VARIANCE FOR ALL RECORDS IS: 0.565644768E-06

RECORD	MEAN	VAR
1	0.0047066	0.462980154E-06
2	0.0044876	0.699376914E-06
3	0.0041754	0.449404467E-06
4	0.0053169	0.497056181E-06
5	0.0048787	0.131611273E-05
6	0.0049228	0.148189002E-06
7	0.0051068	0.409787958E-06
8	0.0058141	0.771185711E-07
9	0.0052923	0.589350861E-06
10	0.0052823	0.391721812E-06
11	0.0032625	0.240969314E-06
12	0.0037546	0.587780164E-06
13	0.0043719	0.383655768E-06
14	0.0044159	0.859961801E-06
15	0.0057757	0.432699494E-06
16	0.0042936	0.742680641E-06
17	0.0046459	0.428550550E-06
18	0.0051466	0.438586566E-06
19	0.0054313	0.708343237E-06
20	0.0050437	0.126560940E-05
21	0.0041554	0.436640221E-06
22	0.0042775	0.185841913E-06
23	0.0040906	0.293477058E-06
24	0.0044285	0.183936550E-06
25	0.0054492	0.172957726E-06
26	0.0039668	0.124956501E-05
27	0.0044500	0.213005023E-06
28	0.0043329	0.347862112E-06
29	0.0041728	0.189060103E-06
30	0.0043480	0.708079142E-06
31	0.0052160	0.248736455E-06
32	0.0043941	0.316722208E-06
33	0.0050374	0.551210292E-06
34	0.0045983	0.299040494E-06
35	0.0038702	0.729812996E-06
36	0.0051866	0.550978712E-06
37	0.0040989	0.388536421E-06
38	0.0040048	0.104349667E-06
39	0.0039631	0.321323796E-06
40	0.0051455	0.251159236E-06

41	0.0044770	0.815714316E-06
42	0.0042206	0.232532102E-06
43	0.0040373	0.322140352E-06
44	0.0048749	0.892711682E-07
45	0.0049881	0.203661187E-06
46	0.0049440	0.172496220E-05
47	0.0053820	0.114750787E-05
48	0.0045014	0.785025804E-06
49	0.0048942	0.756003466E-06
50	0.0041598	0.118347110E-05
51	0.0045313	0.857005375E-06
52	0.0057282	0.718723413E-06
53	0.0053307	0.398412624E-06
54	0.0051968	0.783336645E-06
55	0.0057222	0.426033523E-06
56	0.0053403	0.101901446E-05
57	0.0053577	0.101526053E-05
58	0.0042780	0.853606366E-06
59	0.0042630	0.447939613E-06
60	0.0038458	0.108491622E-05

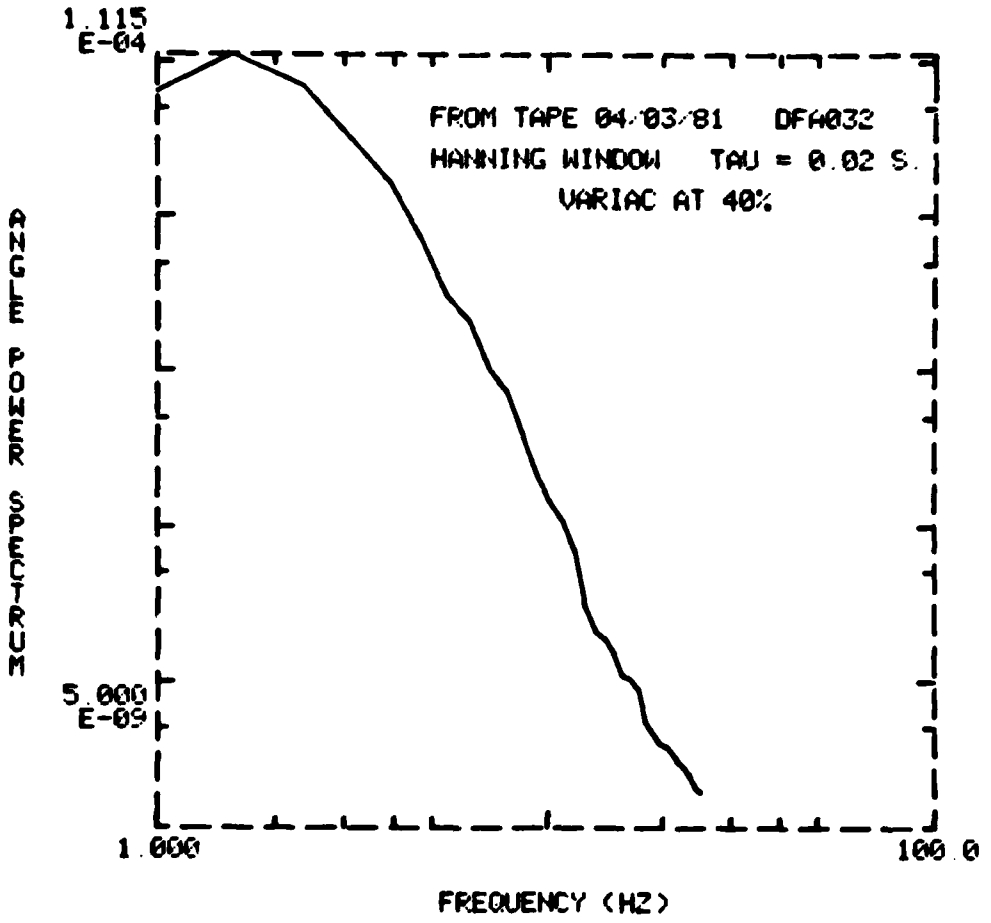

Figure A-3. Power spectrum of angle fluctuations for an input power of 400 watts.

DATA SET #4

Identification # 4/10/81 - DFA102

Input Power: 500 watts

Sampling Time: 20 milliseconds

ANGLE DATA VALUES ARE IN RADIANS. BEAM MADE 5 PASSES. VARIAC @ 50%

ANGLE DATA VALUES ARE IN RADIANS. BEAM MADE 5 PASSES. VARIAC @ 50%
X SCALE FACTOR WAS: 29.245E-06 RAD/UNIT
Y SCALE FACTOR WAS: 18.161E-06 RAD/UNIT
NOISE SUBTRACTED = F, HAMMING WINDOW = T.
ENSEMBLE POWER SERIES COMPUTED AT 16:01:12 ON MON, APR 13 1981
FROM DATA ON TAPE DATED: 04/10/81
SAMPLING INTERVAL IS: 0.0200 SECONDS
60 RECORDS OUT OF 60 WERE USED.
AND 0 WERE BAD
THE AVERAGE VARIANCE FOR ALL RECORDS IS: 0.5738406E-06

RECORD	MEAN	VAR
1	0.0057254	0.926298185E-06
2	0.0048027	0.515414968E-06
3	0.0039309	0.430350838E-06
4	0.0033259	0.262257268E-06
5	0.0051817	0.432688751E-06
6	0.0055831	0.297091219E-06
7	0.0053108	0.318[illegible]4377E-06
8	0.0045475	0.451413066E-06
9	0.0054407	0.704547574E-06
10	0.0048515	0.267491032E-06
11	0.0048586	0.561582738E-06
12	0.0042038	0.671190946E-06
13	0.0041100	0.382905057E-06
14	0.0042897	0.335446259E-06
15	0.0050793	0.[illegible]340[illegible]2E-06
16	0.0049327	0.164496050E-06
17	0.0047265	0.554195936E-06
18	0.0050293	0.255956548E-06
19	0.0039312	0.444986711E-06
20	0.0036356	0.118501298E-05
21	0.0041503	0.380439507E-06
22	0.0037349	0.433173057E-06
23	0.0046933	0.431097874E-06
24	0.0043559	0.695383278E-06
25	0.0036721	0.284550140E-06
26	0.0034011	0.405827507E-06
27	0.0039115	0.695[illegible]9319E-06
28	0.0040330	0.518894467E-06
29	0.0044228	0.906955393E-06
30	0.0044137	0.212850111E-06
31	0.0047685	0.436270057E-06
32	0.0045315	0.662489242E-06
33	0.0044968	0.197578564E-05
34	0.0041550	0.342491603E-06
35	0.0044214	0.661841682E-06
36	0.0046077	0.125172107E-06
37	0.0043260	0.873633212E-06

38	0	0042827	0	576050752E-06
39	0	0034888	0	716394652E-06
40	0	0042518	0	462463674E-06
41	0	0043819	0	967365168E-06
42	0	0042837	0	136965559E-05
43	0	0044258	0	352332449E-06
44	0	0034553	0	12458C561E-05
45	0	0041667	0	429025420E-06
46	0	0033959	0	632916045E-06
47	0	0042150	0	389108834E-06
48	0	0040095	0	136600881E-05
49	0	0042577	0	795778988E-06
50	0	0031981	0	278578455E-06
51	0	0034046	0	320413562E-06
52	0	0048027	0	396059079E-06
53	0	0044654	0	426087013E-06
54	0	0038409	0	796600148E-06
55	0	0044419	0	304040839E-06
56	0	0038249	0	291446668E-06
57	0	0044372	0	656738573E-06
58	0	0042631	0	802522209E-06
59	0	0038342	0	453667858E-06
60	0	0035257	0	558444412E-06

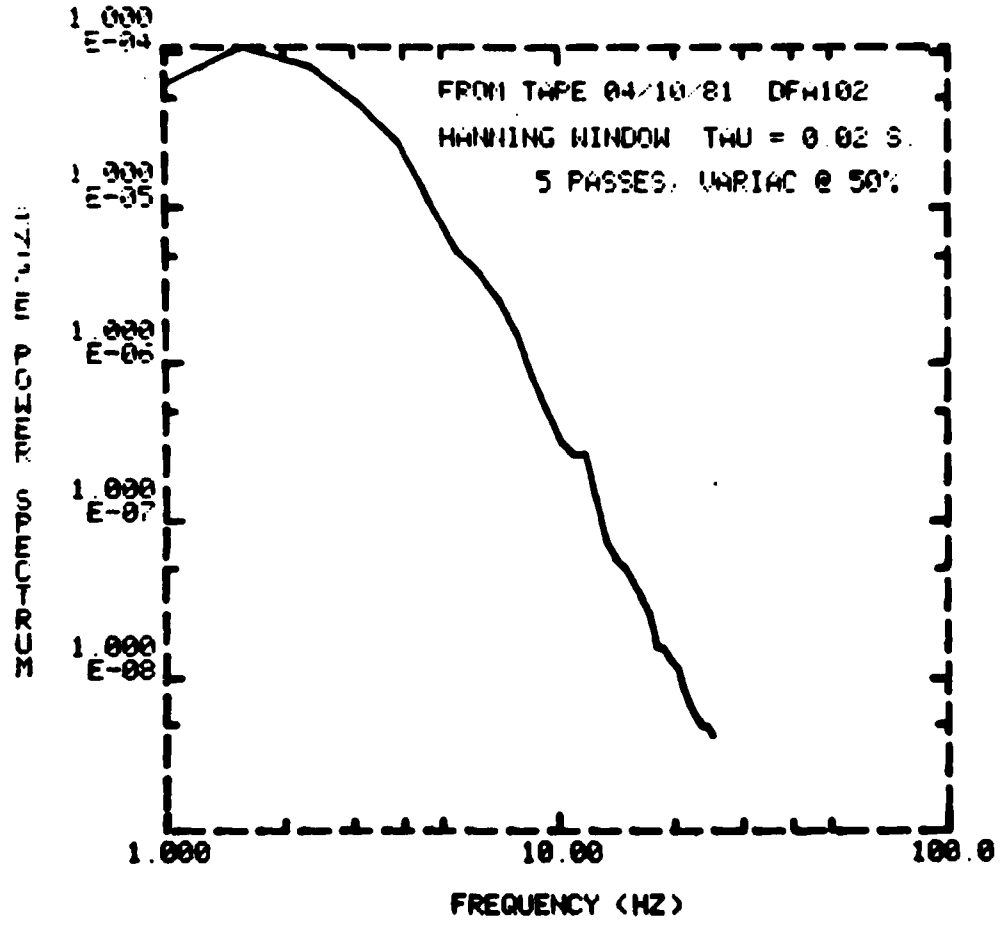

Figure A-4. Power spectrum of angle fluctuations for an input power of 500 watts.

DATA SET #5

Identification # 4/3/81 - DFA033

Input Power: 600 watts

Sampling Time: 20 milliseconds

ANGLE DATA VALUES ARE IN RADIANS.

ANGLE DATA VALUES ARE IN RADIANS.
NOISE SUBTRACTED = F, HANNING WINDOW = T.
ENSEMBLE POWER SERIES COMPUTED AT 15:18:56 ON MON, APR 06 1981
FROM DATA ON TAPE DATED: 04/03/81
SAMPLING INTERVAL IS: 0.0200 SECONDS.
60 RECORDS OUT OF 60 WERE USED,
AND 0 WERE BAD
THE AVERAGE VARIANCE FOR ALL RECORDS IS: 0.269052578E-06

RECORD	MEAN	VAR
1	0.0051924	0.226345378E-06
2	0.0047197	0.236032719E-06
3	0.0043373	0.187720019E-06
4	0.0050932	0.166965265E-06
5	0.0051731	0.339849635E-06
6	0.0055000	0.266004008E-06
7	0.0059151	0.181454368E-06
8	0.0055362	0.309375991E-06
9	0.0045675	0.134603681E-06
10	0.0049507	0.119967524E-06
11	0.0051308	0.949990664E-07
12	0.0050890	0.180889487E-06
13	0.0054233	0.228658706E-06
14	0.0058029	0.116899827E-06
15	0.0052129	0.282158624E-06
16	0.0051568	0.711228040E-06
17	0.0057368	0.615431190E-07
18	0.0051488	0.133246516E-06
19	0.0049612	0.287972910E-06
20	0.0048999	0.102509148E-06
21	0.0049022	0.573387865E-06
22	0.0042763	0.307612424E-06
23	0.0045035	0.669871144E-07
24	0.0046339	0.217450406E-06
25	0.0047547	0.364070274E-06
26	0.0047613	0.270879411E-06
27	0.0041402	0.405728656E-06
28	0.0039665	0.140478761E-06
29	0.0038383	0.209178211E-06
30	0.0040987	0.310725568E-06
31	0.0043928	0.320031347E-06
32	0.0047639	0.473784269E-06
33	0.0047326	0.103362993E-06
34	0.0037849	0.502157604E-06
35	0.0040415	0.718386264E-06
36	0.0052270	0.441665904E-07
37	0.0047033	0.100371665E-06

38	0.0046059	0.267674636E-06
39	0.0042175	0.395378891E-06
40	0.0048222	0.333639548E-06
41	0.0054037	0.901953968E-06
42	0.0043295	0.101091317E-06
43	0.0043244	0.289383991E-06
44	0.0056457	0.743126226E-07
45	0.0057041	0.194524375E-06
46	0.0046873	0.227907066E-06
47	0.0043651	0.287180342E-06
48	0.0042089	0.410809264E-06
49	0.0044822	0.158745905E-06
50	0.0047771	0.245666796E-06
51	0.0049924	0.322665244E-06
52	0.0051331	0.337533379E-06
53	0.0050444	0.250539074E-06
54	0.0052731	0.440314309E-07
55	0.0049708	0.193979588E-06
56	0.0059966	0.277689765E-06
57	0.0057352	0.644506372E-06
58	0.0046010	0.301976627E-06
59	0.0048109	0.795161696E-07
60	0.0052659	0.285276542E-06

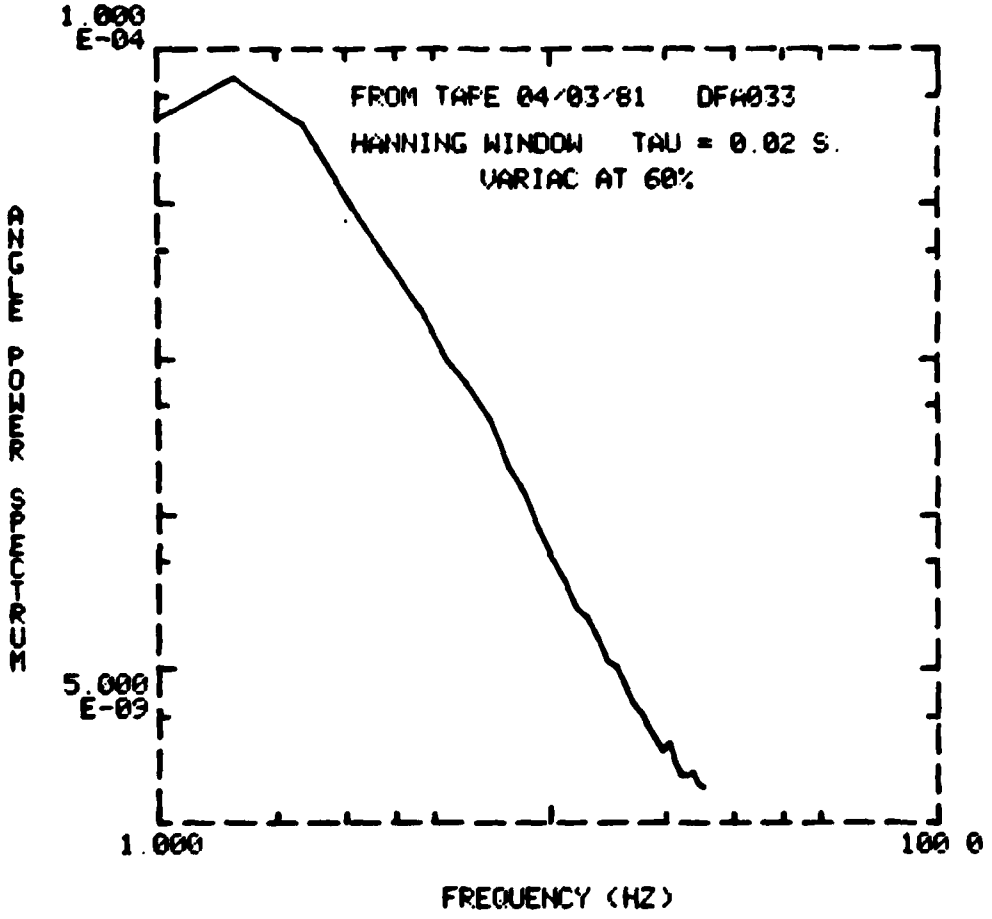

Figure A-5. Power spectrum of angle fluctuations for an input power of 600 watts.

REFERENCES

1. M. T. Tavis and H. T. Yura, "Strong Turbulence Effects on Short Wavelength Lasers," Report SD TR-79-24 prepared for the Air Force Weapons Laboratory, Kirtland Air Force Base, New Mexico.
2. R. A. Elliott, J. R. Kerr, and P. A. Pincus, Appl. Opt. 18, 3315 (1979).
3. R. J. Hill, J. Opt. Soc. Am. 68, 1067 (1978).
4. R. S. Lawrence and J. W. Strohbehn, Proc. IEEE 58, 1523 (1970).

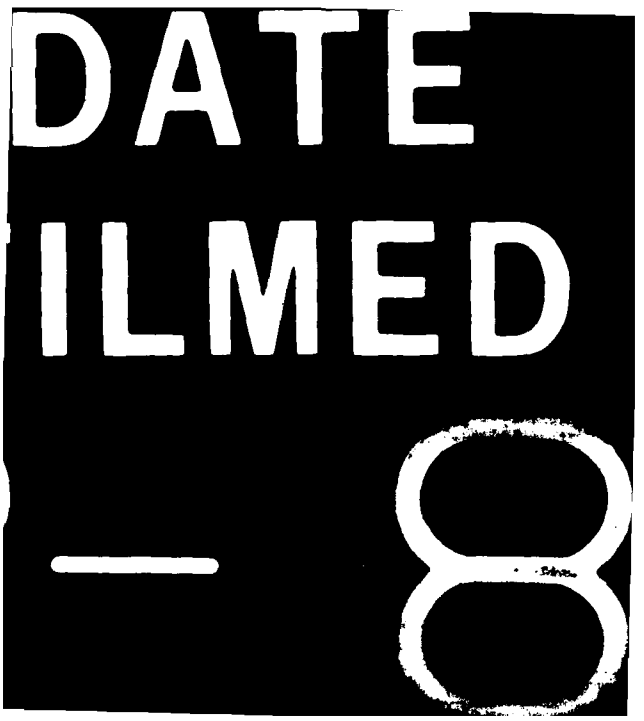
DATE
ILMED
8